Efficient, octave-spanning difference-frequency generation using few-cycle pulses in simple collinear geometry

Hanieh Fattahi,[1,2] Alexander Schwarz,[1,2] Sabine Keiber,[1,2] and Nicholas Karpowicz[1,*]

[1]*Max Planck Institut für Quantenoptik, Hans-Kopfermann-Straße 1, 85748 Garching, Germany*

[2]*Department of Physics, Ludwig-Maximilians-Universität München, Am Coulombwall 1, 85748 Garching, Germany*

**Corresponding author: nicholas.karpowicz@mpq.mpg.de*

Received August 21, 2013; revised September 17, 2013; accepted September 18, 2013;
posted September 19, 2013 (Doc. ID 196144); published October 14, 2013

We present experimental observations and corresponding numerical simulations illustrating the difference-frequency generation of mid-infrared radiation using few-cycle near-infrared-to-visible pulses, which yields conversion efficiencies above 12% in beta-barium borate crystal. Type I and type II phase-matching are shown to yield qualitatively different intensity-scaling behavior, with the former showing higher overall efficiency, especially with the addition of a zero-order wave plate for modifying the polarization state of the pulse, and the latter having a better stability of the spectrum versus input intensity. © 2013 Optical Society of America

OCIS codes: (190.7110) Ultrafast nonlinear optics; (190.4410) Nonlinear optics, parametric processes; (190.4223) Nonlinear wave mixing.

http://dx.doi.org/10.1364/OL.38.004216

Sources of intense, broadband, coherent, and phase-stabilized light in the mid-infrared (MIR) are seeing increasing interest in the ultrafast community, especially in the realm of attosecond physics [1,2]. Both technologically, where the demand for higher photon energies from the high-harmonic-generation process makes longer wavelength-driving pulses advantageous [3–5], and for experiments where either the long wavelength is desirable for avoiding electronic resonances in a solid-state system [6,7] or for matching the oscillations of the applied field to the dynamics being studied [8], there is a great demand for few-cycle MIR light sources. This is now being achieved with optical parametric amplifiers (OPAs), either seeded via difference-frequency generation (DFG) directly in the MIR [9–14] or by utilizing the long-wavelength idler pulse of a near-infrared (NIR) OPA [15–19].

DFG is a popular OPA seed source due to the combination of two properties: the ability to simultaneously phase-match a large fractional bandwidth [20–22] and the intrinsic stability of the carrier-envelope phase (CEP) [17,23] when the signal is derived in a phase-preserving process from the pump. Due to the usually low conversion into the long wavelengths, parametric amplification is used to boost the energy of the MIR pulse. However, there are many experiments where it would be useful to have the MIR pulse precisely synchronized with a NIR or visible pulse, either to use as a pump or a probe. When reaching the microjoule level through a multistage OPA, there is a significant path length, several nonlinear processes and a high-power pump beam all adding complexity and, typically, phase and amplitude noise to any pump-probe experiment. For this reason, simple methods of reaching the MIR with high conversion efficiency would be quite helpful. We show here that a few-cycle visible–NIR pulse obtained from spectral broadening of a commercial Ti:sapphire laser can be used to efficiently obtain broadband pulses in the MIR.

To summarize the experiment, the majority of the output of a nine-pass Ti:sapphire amplifier (FemtoLasers; ~25 fs, 2.8 W at 3 kHz repetition rate) is focused into a 1.1 m hollow-core fiber with 240 μm core diameter, filled with neon gas at a pressure of 2 bar. A white-light continuum emerges from the fiber, with a total power of 1.5 W, and a spectrum from 400 to 1000 nm [24]. This light is compressed using a set of six chirped mirrors [25] and a thin fused silica wedge pair. The compressed pulse duration is below 4 fs, with a total power of 1.0 W in the spectral range 480–1000 nm. The beam was loosely focused by slightly increasing the distance between the end of the fiber and a $f = 1$ m collimating spherical mirror to produce a 0.4 mm FWHM focus ~2 m away. The 500 μm thick, antireflection-coated beta-barium borate crystals (BBOs, Castech) were placed in the laser focus, followed by a collimating mirror, and gold-coated mirrors to either send the beam to a spectrometer (Ocean Optics) or for power measurement. A 2 mm thick antireflection-coated silicon wafer was placed in the beam in order to block the residual short-wavelength light.

The highest conversion efficiency obtained was 12.4%, using type I phase-matching and an additional wave plate inserted in the beam path in order to control the spectrum of the light incident on each axis of the crystal. By tuning the wave plate, a 42 μm quartz plate placed far from the focus and at Brewster's angle, such that the short-wavelength components are predominantly on the fast axis of the BBO, the efficiency of the DFG process is improved. The spectrum obtained corresponding to the highest DFG pulse energy (41 μJ), is shown in Fig. 1(a) alongside the spectrum of the compressed white light pulse after the chirped mirror compressor. Without the wave plate, the efficiency reached 11% for type I and 4.4% for type II. Tighter focusing would result in a filament in air; performing experiments in vacuum with a smaller focus could lead to yet higher conversion efficiencies, since the damage threshold of the BBO was not reached in the measurements.

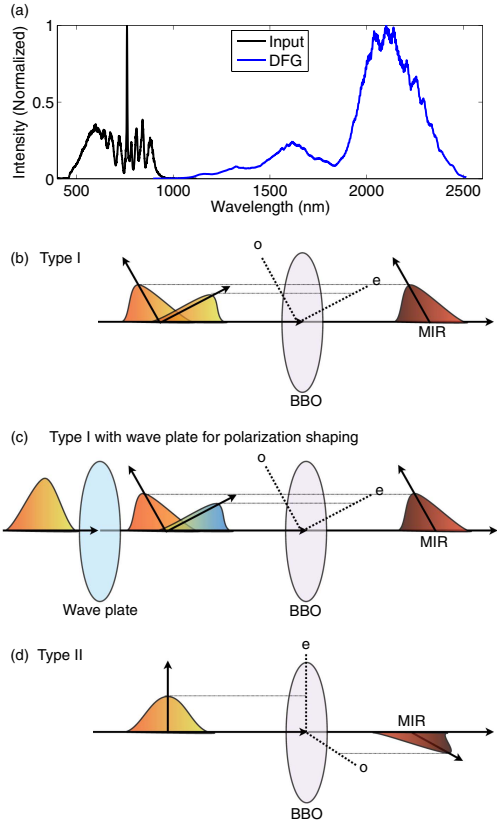

Fig. 1. (a) Input pulse spectrum after chirped mirror compressor and output spectrum of the DFG process showing highest efficiency (see text). (b)–(d) Diagrams of the DFG interactions tested. (b) Type I phase-matching with identical pulses sent to the fast and slow axes of the crystal. (c) Type I phase-matching using a wave plate to send a greater proportion of short-wavelength spectral components to the fast axis. (d) Type II phase-matching with a single, short pulse propagating along the fast axis of the crystal. In all cases, the MIR pulse is created on the slow axis.

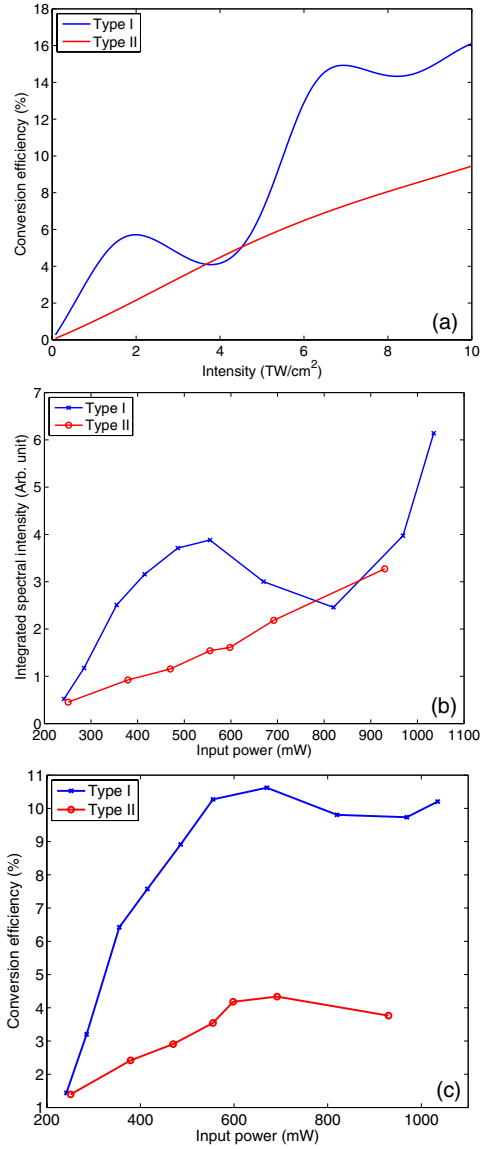

Fig. 2. Power scaling behavior. (a) Simulated conversion efficiency of light into phase-stable, difference-frequency radiation, using 1D propagation in 500 μm thick BBO cut for type I ($\theta = 21.4°$, $\phi = 90°$, light polarization 30° from fast axis) and type II ($\theta = 40°$, $\phi = 0°$). (b) Measured integrated spectral intensity as a function of input power as adjusted with an iris, measured with a beam much larger than the spectrometer entrance slit, indicating the on-axis scaling of the IR radiation. (c) Measured scaling of overall conversion efficiency versus input power.

There are two ways to phase-match the single-pulse DFG process in BBO crystal for broadband output: type I ($e - o \rightarrow o$) and type II ($e - e \rightarrow o$), illustrated in Fig. 1. They exhibit qualitatively different behavior once the energy conversion reaches several percent. In type I DFG, the blue spectral components in the pulse on the fast axis transfer energy to the red components on the slow axis, and, in the process generate a phase-stable idler wave, the DFG output, with the phase-matching condition $k_p - k_s = k_i$, where k_p is the wave vector of the blue wave, k_s is that of the red wave, and k_i is that of the idler. Type II DFG, on the other hand, is similar to optical rectification in the terahertz spectral domain [26]: the nonlinear polarization takes the form of the intensity profile of the pulse, with the alternative phase-matching condition $n_g^{(\mathrm{pump})} = n_o^{(\mathrm{DFG})}$, i.e., the *group* velocity of the pump pulse is equal to the *phase* velocity of the emitted wave. DFG can also be phase-matched in the type II $e - o \rightarrow e$ configuration, but this is not employed here due to its relatively narrow bandwidth.

At low intensities, the efficiency of DFG tends to be linearly proportional to intensity. However, when the conversion efficiency is high, this linearity is broken as the process saturates. Given a long phase-matched interaction length, saturation is reached when energy returns from the MIR pulse to the input pulse through sum-frequency generation faster than it is transferred to it through DFG. Due to the extremely short pulses used here, the effects of group velocity matching result in rather different behavior of the two phase-matching types at high conversion efficiencies. This can be seen both in simulations and experiments in Fig. 2, where the type I process exhibits a clear oscillatory behavior not seen in the type II interaction. The reason for this is straightforward: in type I, the group velocity walk-off between the pulses is much less than in type II.

For example, let us consider the case where the MIR wavelength is 2000 nm, with effective signal and pump wavelengths of 800 and 580 nm. The group indices [27] of DFG, signal and pump are 1.6750, 1.6845, and 1.6932, respectively. This means that the propagation distance in the crystal for a group delay shift of 10 fs between DFG and signal is 315.5 μm, and, for the same shift between signal and pump, the distance is 344.6 μm. In the case of type II phase-matching, the DFG, signal, and pump group indices are 1.6750, 1.6313, and 1.6549, respectively, leading to much shorter distances to separate the DFG from the signal (68.6 μm) and the signal from the pump (127.0 μm). These relatively short length scales reduce the efficiency of the type II process, but at the same time ensure that back-conversion through sum-frequency generation is unlikely at realistic intensities.

Despite the effects of group velocity walk-off in the crystals, the short pulses used in this experiment are important for reaching high conversion efficiencies. Because the damage threshold intensity increases as the pulse duration is decreased, the crystals can be exposed to higher intensities than would be possible with longer pulses [28], compensating for the walk-off effects. When the desired output spectrum is very broadband, short interaction lengths are required in any case.

Higher conversion rates also affect the spectrum obtained through the DFG process. As illustrated in Fig. 3, at the intensity is increased, the type I process exhibits a shift of the peak wavelength of the spectrum, first to longer and then to shorter wavelengths once the local minimum in conversion is reached. The type II process exhibits a more subtle change, gradually adding long-wavelength components at higher intensities, due to the overall redshift of the input pulse as energy is transferred from the short-wavelength side of the input pulse spectrum to the long-wavelength side, shifting the phase-matching to suit lower frequencies. These changes are reproduced by numerical simulations (based on the slowly evolving envelope approximation [29]) including only second-order nonlinearities, indicating that third-order effects are not yet playing a significant role in the process.

The relative stability of the type II process as the input pulse parameters are changed may make it more attractive in many applications, despite its lower conversion efficiency. The fact that the emerging white light and MIR pulses are orthogonally polarized is an advantage: the residual pump light can be nondispersively suppressed, via a Brewster's angle reflection from a silicon wafer, which we found reduces the residual white light contamination level to a few percent, dominated mostly by residual higher-order modes from the hollow-core fiber.

In conclusion, using few-cycle pulses at high intensities in BBO crystal is a promising method for producing broadband MIR pulses for experiments in attosecond and ultrafast science. Conversion efficiencies above 12% can be obtained using type I phase-matching and employing a thin wave plate for spectral polarization control. There are significant differences in the saturation behaviors of the type I and type II phase-matched interactions, which may influence their relative suitability given a specific experimental arrangement. Since only one input pulse, of the type typically already being employed in

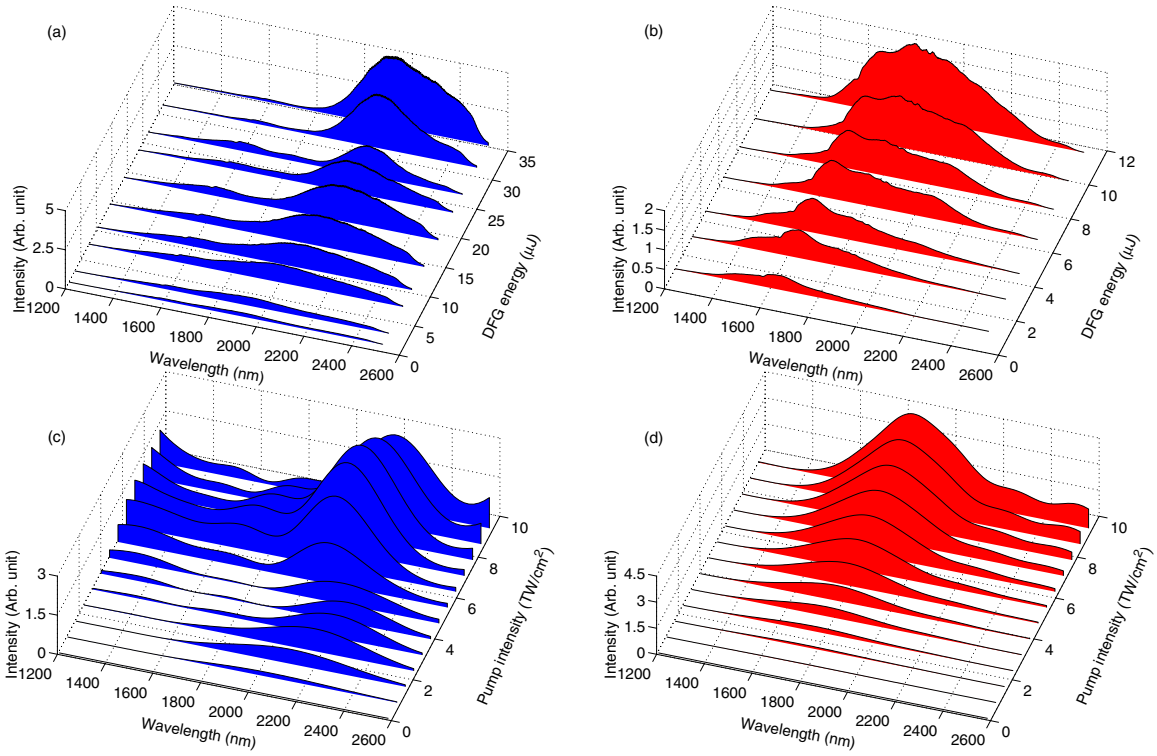

Fig. 3. Difference frequency spectra: (a) and (b) measured spectra for type I (blue) and type II (red) phase-matching, respectively, versus output MIR energy; (c) and (d) corresponding spectra from numerical simulations for type I and type II, respectively. The calculated spectra extend slightly beyond the spectrometer range, but are truncated for comparison.

attosecond beam lines, is required, this technique can be used to easily add an MIR pump or probe pulse to attosecond experiments without the complexity of an additional parametric amplifier.

We gratefully acknowledge helpful discussions with Ferenc Krausz and support from the Munich-Centre for Advanced Photonics, and the German Federal Ministry of Education and Science (BMBP) via the NEXUS project.

References

1. C. Vozzi, M. Negro, and S. Stagira, J. Mod. Opt. **59**, 1283 (2012).
2. K. Schultz, C. Blaga, R. Chirla, P. Colosimo, J. Cryan, A. March, C. Roedig, E. Sistrunk, J. Tate, J. Wheeler, P. Agostini, and L. F. Dimauro, J. Mod. Opt. **54**, 1075 (2007).
3. J. Tate, T. Auguste, H.-G. Muller, P. Salieres, P. Agostini, and L. F. DiMauro, Phys. Rev. Lett. **98**, 013901 (2007).
4. V. Yakovlev, M. Ivanov, and F. Krausz, Opt. Express **15**, 15351 (2007).
5. T. Popmintchev, M.-C. Chen, D. Popmintchev, P. Arpin, S. Brown, S. Alisauskas, G. Andriukaitis, T. Balciunas, O. D. Mucke, A. Pugzlys, A. Baltuska, B. Shim, S. E. Schrauth, A. Gaeta, C. Hernandez-Garcia, L. Plaja, A. Becker, A. Jaron-Becker, M. M. Murnane, and H. C. Kapteyn, Science **336**, 1287 (2012).
6. S. Ghimire, A. D. Dichiara, E. Sistrunk, P. Agostini, L. F. Dimauro, and D. A. Reis, Nat. Phys. **7**, 138 (2010).
7. A. Schiffrin, T. Paasch-Colberg, N. Karpowicz, V. Apalkov, D. Gerster, S. Mühlbrandt, M. Korbman, J. Reichert, M. Schultze, S. Holzner, J. V. Barth, R. Kienberger, R. Ernstorfer, V. S. Yakovlev, M. I. Stockman, and F. Krausz, Nature **493**, 70 (2013).
8. I. Znakovskaya, P. von den Hoff, G. Marcus, S. Zherebtsov, B. Bergues, X. Gu, Y. Deng, M. J. J. Vrakking, R. Kienberger, F. Krausz, R. de Vivie-Riedle, and M. F. Kling, Phys. Rev. Lett. **108**, 063002 (2012).
9. J. Darginavičius, N. Garejev, and A. Dubietis, Opt. Lett. **37**, 4805 (2012).
10. C. Manzoni, C. Vozzi, E. Benedetti, G. Sansone, S. Stagira, O. Svelto, S. D. Silvestri, M. Nisoli, and G. Cerullo, Opt. Lett. **31**, 963 (2006).
11. Y. Deng, A. Schwarz, H. Fattahi, M. Ueffing, X. Gu, M. Ossiander, T. Metzger, V. Pervak, H. Ishizuki, T. Taira, T. Kobayashi, G. Marcus, F. Krausz, R. Kienberger, and N. Karpowicz, Opt. Lett. **37**, 4973 (2012).
12. C. Vozzi, C. Manzoni, F. Calegari, E. Benedetti, G. Sansone, G. Cerullo, M. Nisoli, S. D. Silvestri, and S. Stagira, J. Opt. Soc. Am. B **25**, B112 (2008).
13. K.-H. Hong, S.-W. Huang, J. Moses, X. Fu, C.-J. Lai, G. Cirmi, A. Sell, E. Granados, P. Keathley, and F. X. Kärtner, Opt. Express **19**, 15538 (2011).
14. N. Ishii, K. Kaneshima, K. Kitano, T. Kanai, S. Watanabe, and J. Itatani, Opt. Lett. **37**, 4182 (2012).
15. C. P. Hauri, R. B. Lopez-Martens, C. I. Blaga, K. D. Schultz, J. Cryan, R. Chirla, P. Colosimo, G. Doumy, A. M. March, C. Roedig, E. Sistrunk, J. Tate, J. Wheeler, L. F. Dimauro, and E. P. Power, Opt. Lett. **32**, 868 (2007).
16. F. Silva, P. K. Bates, A. Esteban-Martin, M. Ebrahim-Zadeh, and J. Biegert, Opt. Lett. **37**, 933 (2012).
17. A. Baltuška, T. Fuji, and T. Kobayashi, Phys. Rev. Lett. **88**, 133901 (2002).
18. C. Li, D. Wang, L. Song, J. Liu, P. Liu, C. Xu, Y. Leng, R. Li, and Z. Xu, Opt. Express **19**, 6783 (2011).
19. B. E. Schmidt, A. D. Shiner, P. Lassonde, J.-C. Kieffer, P. B. Corkum, D. M. Villeneuve, and F. Légaré, Opt. Express **19**, 6858 (2011).
20. C. Manzoni, G. Cerullo, and S. D. Silvestri, Opt. Lett. **29**, 2668 (2004).
21. J. Moses, H. Suchowski, and F. Kärtner, Opt. Lett. **37**, 1589 (2012).
22. C. Homann, M. Bradler, M. Förster, P. Hommelhoff, and E. Riedle, Opt. Lett. **37**, 1673 (2012).
23. G. Cerullo, A. Baltuška, O. Mücke, and C. Vozzi, Laser Photon. Rev. **5**, 323 (2010).
24. A. L. Cavalieri, E. Goulielmakis, B. Horvath, W. Helml, M. Schultze, M. Fieß, V. Pervak, L. Veisz, V. S. Yakovlev, M. Uiberacker, A. Apolonski, F. Krausz, and R. Kienberger, New J. Phys. **9**, 242 (2007).
25. V. Pervak, Appl. Opt. **50**, C55 (2011).
26. H. Bakker, G. Cho, H. Kurz, Q. Wu, and X.-C. Zhang, J. Opt. Soc. Am. B **15**, 1795 (1998).
27. K. Kato, IEEE J. Quantum Electron. **22**, 1013 (1986).
28. M. Lenzner, J. Krüger, S. Sartania, Z. Cheng, C. Spielmann, G. Mourou, W. Kautek, and F. Krausz, Phys. Rev. Lett. **80**, 4076 (1998).
29. T. Brabec and F. Krausz, Phys. Rev. Lett. **78**, 3282 (1997).